Protein Subcellular Localization of Fluorescence Imagery using Spatial and Transform domain Features

Muhammad Tahir, Asifullah Khan* and Abdul Majid

Department of Computer and Information Sciences, PIEAS, Islamabad, Pakistan

asif@pieas.edu.pk*

ABSTRACT

Motivation: Subcellular localization of proteins is one of the most significant characteristics of living cells. Prediction of protein subcellular locations is crucial to the understanding of various protein functions. Therefore, an accurate, computationally efficient, and reliable prediction system is required.

Results: In this paper, the predictions of various *SVM* models have been combined through majority voting. The proposed ensemble *SVM-SubLoc* has achieved the highest success rates of 99.7% using hybrid features of Haralick textures and Local Binary Patterns (*HarLBP*), 99.4% using hybrid features of Haralick textures and Local Ternary Patterns (*HarLTP*). In addition, *SVM-SubLoc* has yielded 99.0% accuracy using only Local Ternary Patterns (*LTPs*) based features. The dimensionality of *HarLBP* feature vector is 581 compared to 78 and 52 for *HarLTP* and *LTPs*, respectively. Hence, *SVM-SubLoc* in conjunction with *LTPs* is fast, sufficiently accurate and simple predictive system. The proposed *SVM-SubLoc* approach thus provides superior prediction performance using the reduced feature space compared to existing approaches.

Availability: A web server accompanying the proposed prediction scheme is available at http://111.68.99.218/*SVM-SubLoc*

1 INTRODUCTION

Comprehension of the functions of proteins is of prime importance in the field of biological sciences (Nanni, et al., 2010c). One of the significant characteristics of proteins is its subcellular localization that reveals precious information regarding the working of proteins (Murphy, et al., 2000). Determining protein subcellular locations is significant to the understanding of various protein functions. For instance, during the drug discovery process, precise knowledge of the subcellular localization of proteins can be useful in the identification of drugs. In addition, the effectiveness of drugs can be estimated by knowing the exact locations of proteins before and after using the drugs (Khan, et al., 2011; Srinivasa, et al., 2006).

Fluorescence microscopy is frequently used to determine subcellular localization of proteins in cells. Images of protein locations are normally analyzed in traditional ways, which are time consuming and prone to errors (Chebira, et al., 2007; Nanni, et al., 2010c). Automated approaches are thus required for the classification of such images. These methods need to be computationally efficient and accurate. Fortunately, considerable progress is made in recent years for the development of computational methods that can automatically determine the subcellular protein locations from fluorescence microscopy images (Lin, et al., 2007; Murphy, et al., 2002; Murphy, et al., 2003). Murphy et al. have developed Subcellular Location Feature (*SLF*) sets and trained a back propagation neural network (*BPNN*) to test the performance of these features using *2D HeLa* dataset (Murphy, et al., 2000). Boland and Murphy have tested the performance of Haralick textures, Zernike moments, *SLF1* and different combination of these three by employing the *BPNNs* (Boland and Murphy, 2001). Murphy et al. have trained *BPNN* using enhanced feature sets consisting of Haralick textures, Zernike moments, and morphological features (Murphy, et al., 2003). Hamilton et al. have employed *SVM* using various feature extraction strategies including Threshold Adjacency Statistics (*TASs*), Zernike moments as well as a hybrid of *TASs* and Haralick textures (Hamilton, et al., 2007). Chebira et al. have developed automated classification system for protein subcellular location images in multi-resolution subspaces (Chebira, et al., 2007). They have employed *ANN* at different decomposition levels to obtain the classification results, which are then combined through weight assignment. Nanni et al. have utilized random subspace of Levenberg-Marquardt neural networks and AdaBoost learning algorithm (Nanni, et al., 2009). In addition, they have employed the fusion between these two ensemble classifiers, while different local and global descriptors have been implemented as feature sets. Recently, Nanni et al. have employed a random subspace of Levenberg-Marquardt neural networks using optimized sets of various feature extraction strategies including Wavelet features, Haralick textures, Local Binary Patterns (*LBPs*), Local Ternary Patterns (*LTPs*), and Threshold Adjacency Statistics for *2D HeLa* and *LOCATE* mouse protein datasets (Nanni, et al., 2010a).

The models proposed by different researchers have still margin in improving the prediction accuracy and reducing the dimensionality of the feature space. The aim of this study is to develop an accurate and simple system compared to the existing approaches. We thus develop both individual and hybrid features based classification approaches for the prediction of protein subcellular localization. In the proposed approach, we employ Haralick textures, Zernike moments, *LBPs*, *LTPs*, and *TASs* based feature extraction strategies. Different hybrid feature sets are formed by concatenating these features. The performance of various kernels of *SVM* has been investigated using these features. To enhance the performance of the proposed model, the success rates of different *SVMs* have been combined through majority voting. Discrete Wavelet Transforms is used for the extraction of Haralick textures and Zernike moments only. For this purpose, we have decomposed

*To whom correspondence should be addressed.

the image up to four levels so that the best decomposition level could be detected. Then, we have used statistical measures to acquire Haralick textures and Zernike moments from each decomposed image.

Rest of the paper is organized as follows: Dataset and different feature extraction strategies are described in Section 2. The proposed approach is presented in Section 3. Results and discussions are elaborated in Section 4. Conclusions are drawn at the end.

2 METHODS

2.1 Dataset

Three datasets have been used to evaluate the performance of our proposed scheme including *2D HeLa*, LOCATE Endogenous, and LOCATE Transfected datasets. The *2D HeLa* dataset contains 862 single-cell images, each of size 382 x 382, distributed in 10 classes (Chebira, et al., 2007). LOCATE Endogenous and LOCATE Transfected datasets contain 502 and 553 images, respectively. Each image is of size 768 x 512, having up to 13 cells. LOCATE Endogenous and LOCATE Transfected images are distributed in 10 and 11 classes, respectively (Nanni, et al., 2010a). Classes and images per each class of *2D HeLa* and LOCATE datasets are provided in supplementary Tables 12 and 13, respectively.

2.2 Feature Extraction Strategies

In this work, we have employed various texture based feature extraction strategies such as Haralick textures, Zernike moments, *LBPs*, *LTPs*, and *TASs*. We describe these feature extraction strategies as follows.

2.2.1 Haralick Texture Features

Haralick features are texture based statistical measures utilized by a number of researchers for classification (Hamilton, et al., 2006; Haralick, 1979; Nanni, et al., 2010c). A Spatial Gray Level Dependence Matrix (*SGLD*) of size N x N is first obtained for an image with N gray levels at certain angle θ (i.e. 0°, 45°, 90° and 135°) at some distance d, where d is measured in terms of pixel distance. In this work, d is set to one. Then thirteen statistical measures are calculated from *SGLD* matrix, namely energy, correlation, inertia, entropy, inverse difference moment, sum average, sum variance, sum entropy, difference average, difference variance, difference entropy, and two information measures of correlation. In this work, features along horizontal and vertical directions are combined by averaging. Similarly, features along diagonal and off-diagonal directions are also combined by averaging. As a result, we have obtained a total of 26 features for each image without Discrete Wavelet Transform (*DWT*). With *DWT*, the number of images at each decomposition level varies as well as the dimension of feature space as shown in Table 1.

2.2.2 Zernike Moment based Features

A set of complex polynomials, which form a complete orthogonal set over the interior of the unit circle, provides the basis to compute Zernike moments. Zernike moments do not bear redundant information between the moments because Zernike polynomials are orthogonal to each other. They are computationally inexpensive compared to other texture based features (Hu and Murphy, 2004). Zernike moments of an image can be calculated using Equation 1 (Boland, et al., 1998).

$$Z_{nl} = \frac{n+1}{\pi} \sum_{x,y} V_{nl}^{*}(x,y) I(x,y) \tag{1}$$

where $I(x, y)$ represents the pixel intensity at position (x, y), $x^2 + y^2 \le 1, 0 \le l \le n, n - l$ is even. V_{nl}^{*} indicates complex conjugate of the Zernike Polynomial of degree n and angular dependence. Its value can be computed as follows:

$$V_{nl}(x,y) = \sum_{m=0}^{(n-l)/2} \frac{(-1)^m (x^2+y^2)^{n/2-m} e^{il\theta} (n-m)!}{m!(\frac{n-2m+l}{2})!(\frac{n-2m-l}{2})!} \tag{2}$$

where $0 \le l \le n, n - l$ is even and $\theta = \tan^{-1}(y/x)$.

In this work, we have obtained Zernike moments of order 12 as used by (Boland, et al., 1998; Chebira, et al., 2007; Hamilton, et al., 2007). These features are extracted in spatial and transform domains. We have employed *DWT* for the transformation, which decomposes each image into four sub-images. We have computed features at each decomposition level separately. Due to the varying number of images at each decomposition level, dimensions of feature vectors also vary as shown in Table 2.

2.2.3 Local Binary Patterns (*LBPs*)

Local Binary Patterns is a texture based feature extraction strategy for gray level patterns in an image, proposed by (Ojala, et al., 1996). *LBPs* operator evaluates the binary differences between the gray value of the central pixel c and the gray values of P pixels in the neighborhood on a circle of radius R around c (Nanni, et al., 2010a; Nanni, et al., 2010b; Nanni and Lumini, 2008). The procedure of obtaining *LBPs* code is depicted in Figure 1.

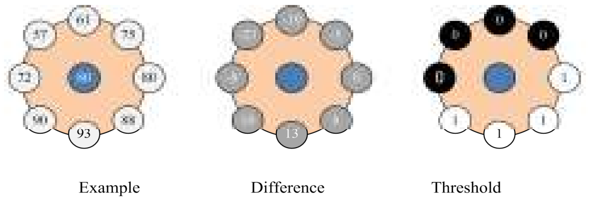

$1 * 2^0 + 1 * 2^1 + 1 * 2^2 + 1 * 2^3 + 0 * 2^4 + 0 * 2^5 + 0 * 2^6 + 0 * 2^7 = 15 \quad s(x) = \begin{cases} 1, & \text{if } x \geq 0 \\ 0, & \text{otherwise} \end{cases}$

Figure 1 Procedure of *LBPs* code generation

s(x) shows the value of each pixel *p* after applying the threshold. The *LBPs* code is generated according to Equation 3:

$$LBP_{P,R} = \sum_{p=0}^{P-1} s(g_p - g_c)2^p \tag{3}$$

Where g_c and g_p represent the gray-level values of central and neighboring pixels, respectively. *LBPs* are computed using uniform (*u2*), rotation invariant (*ri*), and uniform rotation invariant (*riu2*) mappings on three different configurations: (*R*=1, *N*= 8), (*R*=2, *N*=16), and (*R*=3, *N*=24) where *R* and *N* indicate radius and neighborhood, respectively.

2.2.4 Local Ternary Patterns (*LTPs*)

LTPs is based on the generalization of *LBPs* (Tan and Triggs, 2007). In *LTPs*, the difference between a central pixel *c* and its neighbor *u* is based upon a ternary value according to a threshold θ as given by Equation 4.

$$s(u) = \begin{cases} 1 & if \ u \geq c + \theta \\ -1 & if \ u \leq c - \theta \\ 0 & otherwise \end{cases} \tag{4}$$

To reduce computational complexity, the ternary pattern is split into two binary patterns according to its positive and negative components, as shown in Figure 2. The histograms computed from the component binary patterns are concatenated to obtain the feature vector for the ternary pattern (Nanni, et al., 2010a; Nanni, et al., 2010b).

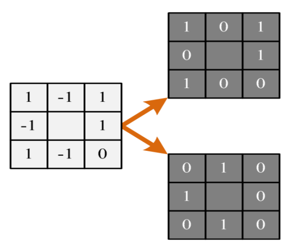

Figure 2 *LTP* code splits into two *LBP* codes

LTPs are also computed using uniform (*u2*), rotation invariant (*ri*), and uniform rotation invariant (*riu2*) mappings on three different configurations i.e. (*R*=1, *N*= 8), (*R*=2, *N*=16), and (*R*=3, *N*=24) where *R* and *N* indicate value of radius and number of neighborhood pixels, respectively.

2.2.5 Threshold Adjacency Statistics (*TASs*)

Threshold Adjacency Statistics (*TASs*) based features are computationally inexpensive and efficient metric for classifying subcellular localization images (Hamilton, et al., 2007). *TASs* features are computed from three 9-bin histograms, obtained from three different binary images, generated using three different thresholds (Nanni and Lumini, 2008). These features are calculated as follows. First, a threshold is applied to the image to produce a binary image. Then, nine statistics are computed from that binary image as shown in Figure 3.

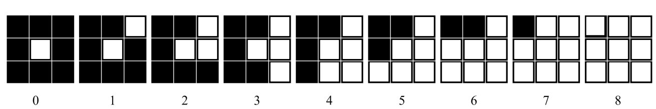

Figure 3 Threshold Adjacency Statistics: 0 to 8 neighboring white pixels of a central white pixel in a 3 x 3 neighborhood

The first statistic is the number of white pixels that have no white neighbors, the second statistic is the number of white pixels that have exactly one white neighbor, and the third statistic is the number of white pixels that have exactly two white neighbors. This process is repeated up to eight white neighboring pixels for 8-bit gray scale image. Two other sets of *TASs* are calculated in similar fashion. Each set of *TAS* is computed for binary images with pixel intensities in the range of μ to 255, μ - θ to 255, and μ + θ to 255 where μ is the average pixel intensity and θ is the user defined threshold. The value of threshold θ

should not be less than 30 since less values are considered as background intensities (Hamilton, et al., 2007). We have observed the best results when θ = 140 as shown in Table 3.

2.2.6 Hybrid Features

A hybrid feature model is produced by combining different individual features to enhance the discrimination power of the feature space. The hybrid features include *ZHar* (Zernike + Haralick), *HarLBP* (Haralick + *LBPs*), *HarLTP* (Haralick + *LTPs*), and *HarTAS* (Haralick + *TASs*). Only *ZHar* hybrid features are formed both in spatial and transform domains.

2.3 Support Vector Machine (*SVM*)

SVM is a popular machine learning technique used in the field of pattern recognition and classification. The theoretical detail of *SVM* is available in the machine learning literature (Gunn, 1998; Hayat and Khan, 2010; Majid, et al., 2006). It was developed for binary classification problems. However, to employ *SVM* for multi-classification problems, a straightforward approach is to reduce the multi-classification to a series of binary classifications through one-versus-rest mechanism. For a *k*-class classification problem, *k SVMs* are built where the i^{th} *SVM* is trained on every instance in the i^{th} class with positive labels and all other instances with negative labels. In this study, we have used four different kernels; linear (*lin*), polynomial (*poly*) of degree 2, Radial Basis Function (*RBF*), and sigmoid (*sig*).

2.4 The Proposed *SVM-SubLoc* Approach

The framework of our proposed approach is shown in Figure 4. This figure highlights a new prediction model *SVM-SubLoc* based on different individual and hybrid feature sets. Individual features, such as Haralick textures and Zernike moments are extracted in transform and spatial domains using *DWT*. However, Local Binary Patterns, Local Ternary Patterns, and Threshold Adjacency Statistics are obtained in spatial domain only. Hybrid features are constructed by concatenating these features in different combinations as described in section 2.2.6. The performance of various *SVMs* has been evaluated using these features. The predictions of these *SVMs* have been combined through majority voting to improve the performance of the proposed model. In case of a tie among the individual classifiers' voting, preference is given to the classifier with the highest performance.

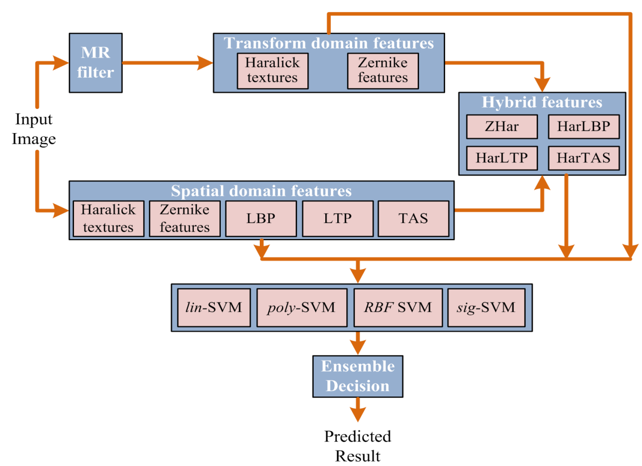

Figure 4 Framework of the proposed *SVM-SubLoc*

3 RESULTS AND DISCUSSIONS

The Jackknife test is the most accurate and significantly efficient method for measuring the performance of algorithms (Hamilton, et al., 2007; Khan, et al., 2008). We have applied 5-fold cross validation to explore the performance of the proposed approach. In case of *2D HeLa*, due to the slight imbalance, the input data is stratified before applying the cross validation. The analysis of the results for *2D HeLa* dataset is presented in section 3.1. The features that performed well on *2D HeLa* have also been tested on LOCATE Endogenous and Transfected datasets. In section 3.2, only the best results on the two LOCATE datasets have been reported. However, detailed analysis using *LTPs*, *HarLBP*, and *HarLTP* is provided in the supplementary material. We have used Accuracy, *F*-Score, *MCC*, and *Q*-Statistic as performance measures.

$$Q_{avg} = \frac{2}{L(L-1)} \sum_{i=1}^{L-1} \sum_{k=i+1}^{L} Q_{i,k} \tag{5}$$

3.1 Performance Analysis for *2D HeLa* dataset

We have computed the aforementioned measures using individual and hybrid features for *2D HeLa* dataset. In this section, first, we discuss the performance of *SVM-SubLoc* using individual feature sets on *2D HeLa* dataset. Afterwards, the performance of *SVM-SubLoc* will be reported for hybrid feature sets.

3.1.1 Performance of *SVM-SubLoc* using Individual Feature sets

In this section, we discuss our findings about the performance of *SVM-SubLoc* using individual features constructed in Section 2.2.

a. Performance of *SVM-SubLoc* using Haralick Texture Features

Table 1 shows the performance of *SVM-SubLoc* using Haralick textures with/without *DWT*. Here, *L* and *D* represent the decomposition level and dimension of the feature vector, respectively.

Table 1 Performance of *SVM-SubLoc* using Haralick Texture Features with/without *DWT*

		lin	*poly*	*RBF*	*sig*	Ensemble			
L	*D*	Acc				Acc	*MCC*	*F*-Score	*Q*-Statistic
0	26	75.6	75.9	76.4	69.6	87.7	0.59	0.60	0.29
1	104	80.5	80.9	81.7	80.3	92.5	0.71	0.72	**0.18**
2	416	81.9	83.2	**84.1**	79.8	**93.2**	**0.73**	**0.74**	0.20
3	1664	77.3	78.3	80.6	77.9	90.2	0.65	0.66	0.30
4	6656	79.5	80.6	80.7	79.5	92.6	0.72	0.73	0.23

The individual *RBF-SVM* has achieved the highest success rates at all decomposition levels. Particularly, its highest accuracy 84.1% is observed at 2nd decomposition level. Further, the *SVM-SubLoc* has brought a significant improvement in the prediction of subcellular protein locations for *2D HeLa* dataset. *SVM-SubLoc* has achieved the highest accuracy 93.2%, which is 9.1% higher than that of *RBF-SVM*. This shows that 2nd level is the best decomposition level for this dataset. This is because at lower decomposition levels some valuable hidden information is lost. However, at higher decomposition levels, we obtained redundant information, which degraded the performance of the classifiers. The highest *MCC* value at 2nd level shows that the prediction is quite encouraging. Similarly, the highest *F*-Score value at this level indicates the best accuracy at this level. On the other hand, the highest diversity is obtained at 1st decomposition level with the *Q* value 0.18.

b. Performance of *SVM-SubLoc* using Zernike moment based Features

The predictions of *SVM-SubLoc* using Zernike moments are reported in Table 2 with/without *DWT*.

Table 2 Performance of *SVM-SubLoc* using Zernike moment based Features with/without *DWT*

		lin	*poly*	*RBF*	*sig*	Ensemble			
L	*D*	Acc				Acc	*MCC*	*F*-Score	*Q*-Statistic
0	49	28.3	43.8	46.5	15.5	46.7	-0.02	0.16	0.02
1	196	35.9	50.3	52.2	24.4	57.8	0.12	0.23	0.09
2	784	39.0	53.4	56.2	15.1	**58.5**	**0.15**	**0.25**	**0.01**
3	3136	50.2	52.0	60.5	11.3	54.5	0.10	0.22	0.24
4	12544	44.0	48.0	**67.8**	11.0	56.7	0.14	0.24	0.11

At 0th decomposition level, the highest yielded accuracy is 46.5%, which indicates poor feature extraction at that level. Among the base classifiers, *sig-SVM* has shown poor performance; only the accuracy of *RBF-SVM* is improved with the increase in the decomposition levels. We achieved the highest accuracy 67.8% at 4th level. Though, *SVM-SubLoc* has yielded the best accuracy 58.5% at 2nd level due to the maximum diversity at this level as indicated by the *Q* value 0.01. However, prediction quality and accuracy of the test are not reasonably good as shown by the *MCC* and *F*-Score values at 2nd decomposition level.

c. Performance of *SVM-SubLoc* using *TASs*

Table 3 demonstrates the predictions of *SVM-SubLoc* using *TASs* for gray images without *DWT*.

Table 3 Performance of *SVM-SubLoc* using Threshold Adjacency Statistics

		lin	*poly*	*RBF*	*sig*	Ensemble			
θ	*D*	Acc				Acc	*MCC*	*F*-Score	*Q*-Statistic
140	27	77.6	80.3	**81.0**	70.7	**91.6**	**0.69**	**0.70**	**0.31**

In individual base classifiers, *RBF-SVM* has achieved the highest accuracy 81.0% compared to other *SVMs*. The success rate of *SVM-SubLoc* is 91.6%, which is 10.5% higher than that of *RBF-SVM*. The increased ensemble accuracy shows the significance of the ensemble classifier. *MCC* value 0.69 shows good quality of the prediction whereas *F*-Score value 0.70 indicates fine accuracy of the performed test. The *Q* value 0.31 reveals that results have 69% diversity. It has been analyzed during the experiments that *TASs* have produced the most significant results for θ = 140. The discriminating capability of these features at this threshold is enhanced. The results achieved at other threshold values are presented in supplementary Table 1 for comparison.

d. Performance of *SVM-SubLoc* using *LBPs*

The predicted outcomes of *SVM-SubLoc* using *LBPs* are presented in Table 4. Here, *m* represents mapping.

In individual base learners, *RBF-SVM* has achieved the highest accuracy 88.0% using riu2 *LBPs* for *R*=3 and *N*=24. However, *SVM-SubLoc* has yielded the highest accuracy 95.5% using *u2 LBPs* for *R*=3 and *N*=24. The performance accuracy of *SVM-SubLoc* is 7.5% higher than that of *RBF-SVM*, which highlights the significance of the proposed ensemble technique. The maximum diversity of *SVM-SubLoc* has been observed when the features are extracted on the circle of radius 3 as is evident from *Q* value 0.25. The best values of *MCC* (= 0.81) and *F*-Score (= 0.82) are also obtained using *u2 LBPs*.

e. Performance of *SVM-SubLoc* using *LTPs*

In Table 5, the success rates of *SVM-SubLoc* using *LTPs* are shown for gray images without *DWT*. There is an additional parameter θ used by *LTPs*, which defines the threshold. In individual classifiers, *poly-SVM* has achieved the highest accuracy 94.4% for *R*=3, *N*=24, and θ=80 using *riu2 LTPs*. The highest accuracy 99.0% achieved by *SVM-SubLoc* is 4.6% higher than that of *poly-SVM*. It has been investigated that *LTPs* have more discriminative capability compared to other feature sets. As is evident from the *Q* value 0.15, we observed the maximum diversity using *riu2 LTPs* for *R*=3 and *N*=24 and that is the main reason why the ensemble accuracy is high. An *MCC* value 0.95 and *F*-Score value 0.95 also indicate that discrimination power *of riu2 LTPs* is better. It is evident from Table 5 that threshold values vary at *R* =1 and *R*=2, 3. At smaller circles, the small value of θ performs well. However, at larger circles, the value of θ should be greater.

Table 4 Performance of *SVM-SubLoc* using Local Binary Patterns (*LBPs*) for various mappings

				lin	***poly***	***RBF***	***sig***	**Ensemble**			
R	*N*	*m*	*D*	Acc				Acc	*MCC*	*F*-Score	*Q*-Statistic
1	8	u2	59	83.7	84.3	85.3	71.5	92.8	0.72	0.73	0.32
1	8	ri	36	83.5	82.4	82.7	72.9	92.8	0.72	0.73	0.34
1	8	riu2	10	81.5	82.5	82.5	74.9	92.5	0.71	0.72	0.33
2	16	u2	243	85.7	86.8	87.5	78.6	95.0	0.79	0.80	0.32
2	16	ri	4116	73.2	72.6	73.0	70.5	85.4	0.54	0.56	0.37
2	16	riu2	18	87.1	86.8	87.8	78.3	95.1	0.79	0.80	0.37
3	24	u2	555	85.0	86.3	87.4	78.8	**95.5**	**0.81**	**0.82**	**0.25**
3	24	riu2	26	85.7	86.4	**88.0**	80.5	94.8	0.78	0.79	0.34

Table 5 Performance of *SVM-SubLoc* using Local Ternary Patterns (*LTPs*) for various mappings

					lin	***poly***	***RBF***	***sig***	**Ensemble**			
R	*N*	θ	*m*	*D*	Acc				Acc	*MCC*	*F*-Score	*Q*-Statistic
1	8	40	u2	118	90.4	90.4	90.8	78.1	97.7	0.89	0.90	0.35
1	8	40	ri	72	89.3	87.5	89.3	80.5	97.3	0.87	0.88	0.28
1	8	40	riu2	20	89.2	89.7	90.1	77.2	97.3	0.87	0.88	0.28
2	16	80	u2	486	92.8	93.0	92.9	84.1	98.2	0.91	0.92	0.21
2	16	80	riu2	36	91.8	92.9	93.5	85.1	98.6	0.93	0.93	0.26
3	24	80	riu2	52	93.8	**94.4**	93.8	86.3	**99.0**	**0.95**	**0.95**	**0.15**

3.1.2 Performance of *SVM-SubLoc* using Hybrid Feature Sets

In this section, we discuss our findings regarding *SVM-SubLoc* using hybrid feature sets as given in Section 2.2.6.

a. Performance of *SVM-SubLoc* using *ZHar*

In Table 6, we present the predicted accuracies of *SVM-SubLoc* using the hybrid of Zernike and Haralick texture features with/without *DWT*. In individual classifiers, we have found the best performance of 80.8% for *RBF-SVM*.

Table 6 Performance of *SVM-SubLoc* using *ZHar* with/without *DWT*

		lin	***poly***	***RBF***	***sig***	**Ensemble**			
L	*D*	Acc				Acc	*MCC*	*F*-Score	*Q*-Statistic
0	75	69.7	69.7	71.8	57.5	84.4	0.52	0.54	0.19
1	300	74.8	76.2	76.9	74.4	90.4	0.66	0.67	**0.12**
2	1200	80.0	80.5	**80.8**	77.2	**93.2**	**0.73**	**0.74**	0.24
3	4800	77.3	77.9	78.5	77.4	89.2	0.62	0.64	0.35
4	19200	77.8	80.0	79.3	76.2	90.8	0.66	0.68	0.33

The highest accuracy 93.2% obtained by *SVM-SubLoc* is 12.4% higher than that of *RBF-SVM*. The 2nd decomposition level has been found to be the best level for discriminating subcellular location images. However, most diverse results are obtained at 1st level as indicated by Q value 0.12. Highest values of *MCC* 0.73 and *F*-Score 0.74 are also achieved at 2nd level, which show that both quality of prediction and accuracy of the test are best at this level. The individual classifiers using these hybrid features do not produce better results compared to using their individual constituents. However, *SVM-SubLoc* has yielded the same accuracy as yielded by the ensemble using Haralick textures.

b. Performance of *SVM-SubLoc* using *HarTAS*

The success rates of *SVM-SubLoc* using *HarTAS* have been given is Table 7. Among different kernel based *SVMs*, *poly-SVM* has achieved the highest accuracy 87.9%, which is further enhanced by the ensemble *SVM-SubLoc* up to 96.2%.

Table 7 Performance of *SVM-SubLoc* using *HarTAS*

		lin	*poly*	*RBF*	*sig*	Ensemble			
θ	*D*	Acc				Acc	*MCC*	*F*-Score	*Q*-Statistic
140	53	87.0	**87.9**	86.0	83.0	**96.2**	**0.83**	**0.84**	**0.32**

This shows 8.3% improvement in the accuracy. The Q value 0.32 indicates sufficient diversity among classifiers. Quality of the prediction and accuracy of the test are quite good as revealed by MCC value 0.83 and F-Score value 0.84, respectively. The results at other threshold values are presented in supplementary Table 2.

c. Performance of *SVM-SubLoc* using *HarLBP*

The results of *SVM-SubLoc* using hybrid feature set of *HarLBP* are shown in Table 8. In individual classifiers, *RBF-SVM* has achieved the highest accuracy 94.4% for R=3 and N=24. The obtained accuracy is 17.9% higher than the highest accuracy using Haralick textures (at 0th level) as given in Table 1 and 6.3% higher than the highest accuracy using *LBPs* as shown in Table 4 using the same kernel. The *SVM-SubLoc* has yielded 99.7% accuracy, which is 5.3% higher than that of *RBF-SVM*. It has been observed that *u2 LBPs*, computed on a larger circle and concatenated with Haralick textures, gives more discrimination power to the classifier. *MCC* and *F*-Score values 0.98 each indicate that both the quality of prediction and accuracy of test are admirable when Halick textures are concatenated with *u2 LBPs* for R=3 and N=24. However, diverse results are obtained when Haralick textures are concatenated with *u2 LBPs* on circles of radius 1 and 2 as indicated by Q value 0.14.

Table 8 Performance of *SVM-SubLoc* using *HarLBP*

				lin	*poly*	*RBF*	*sig*	Ensemble			
R	*N*	*m*	*D*	Acc				Acc	MCC	*F*-Score	*Q*-Statistic
1	8	u2	85	92.1	92.4	92.5	88.5	99.3	0.96	0.96	**0.14**
1	8	ri	62	89.2	89.9	89.0	84.9	97.0	0.86	0.87	0.31
1	8	riu2	36	88.3	90.2	89.6	87.9	97.5	0.88	0.89	0.28
2	16	u2	269	93.2	93.9	**94.4**	91.7	99.0	0.95	0.95	**0.14**
2	16	ri	4142	81.6	81.6	78.5	81.0	92.5	0.71	0.72	0.28
2	16	riu2	44	92.5	93.2	93.7	90.8	98.8	0.94	0.94	0.18
3	24	u2	581	93.2	93.6	**94.4**	90.9	**99.7**	**0.98**	**0.98**	0.20
3	24	riu2	52	91.8	92.6	92.8	89.7	99.3	0.96	0.96	0.34

Table 9 Performance of *SVM-SubLoc* using *HarLTP*

					lin	*poly*	*RBF*	*sig*	Ensemble			
R	*N*	θ	*m*	*D*	Acc				Acc	MCC	*F*-Score	*Q*-Statistic
1	8	40	u2	144	92.4	92.5	92.2	85.2	98.1	0.91	0.91	0.24
1	8	40	ri	98	90.9	90.6	90.3	87.8	98.3	0.92	0.92	0.30
1	8	40	riu2	46	88.8	91.5	91.8	88.2	98.2	0.91	0.92	0.19
2	16	80	u2	512	94.3	**94.7**	94.4	92.3	99.0	0.95	0.95	0.07
2	16	80	riu2	62	93.2	93.1	93.6	90.7	99.0	0.95	0.95	0.19
3	24	80	riu2	78	93.9	93.9	93.1	90.8	**99.4**	**0.97**	**0.97**	**0.05**

d. Performance of *SVM-SubLoc* using *HarLTP*

The predictions of *SVM-SubLoc* using *HarLTP* have been presented in Table 9. In individual classifiers, *poly-SVM* has yielded the highest accuracy 94.7% using the hybrid of Haralick textures and *u2 LTPs* for R=2, N=16, and θ=80. The ensemble *SVM-SubLoc* has achieved the highest accuracy 99.4% using the hybrid of Haralick textures and *riu2 LTPs* for R=3, N=24, and θ=80. The ensemble has yielded 4.6% higher accuracy than that of *poly-SVM*. *MCC* and *F*-Score have yielded the highest values for the hybrid of Haralick and *riu2 LTPs* for

R=3, N=24, and θ=80. It means that prediction quality and test accuracy are promising. Maximum diversity is achieved using *HarLTP* as shown by Q value 0.05.

3.2 Performance Analysis for LOCATE dataset

In this section, Table 10 reports the performance predictions of *SVM-SubLoc* using *LTPs*, *HarLBP*, and *HarLTP* features on LOCATE Endogenous and Transfected datasets. Only the best ensemble outcomes are shown here.

Table 10 Highest Ensemble Accuracies achieved using LOCATE Endogenous and Transfected datasets

Dataset	*Feature*	*Ensemble Accuracy*	*MCC*	*F-Score*	*Q-Statistic*
Endogenous	HarLBP	**99.8**	0.98	0.99	0.10
Transfected	HarLTP	**98.7**	0.92	0.93	0.20

The complete results using these three feature sets are given in supplementary Tables 6, 7, 8, 9, 10, and 11. The *SVM-SubLoc* has achieved the highest accuracy of 99.8% using *HarLBP* features for LOCATE Endogenous dataset. However, *SVM-SubLoc* has yielded 98.7% accuracy using *HarLTP* for LOCATE Transfected dataset.

3.3 Comparison with existing Approaches

In Table 11, we have carried out a performance comparative analysis of the proposed *SVM-SubLoc* approach with previously well-known approaches for *2D HeLa* and the two LOCATE datasets.

The accuracy 95.4% is obtained by the proposed approach for *2D HeLa* dataset in (Chebira, et al., 2007). Nanni and Lumini have reported accuracies of 94.2%, 98.4%, and 96.5% for the *2D HeLa*, LOCATE Endogenous and Transfected datasets, respectively (Nanni and Lumini, 2008). In an another paper, Nanni et al. have reported the highest accuracy 97.5% for *2D HeLa* dataset (Nanni, et al., 2010c). Nanni et al. have also reported 95.8% accuracy for *2D HeLa* dataset, 99.5% for LOCATE Endogenous, and 97.0% accuracy for LOCATE Transfected dataset (Nanni, et al., 2010a). On the other hand, our proposed *SVM-SubLoc* approach has yielded 99.7% accuracy using *HarLBP* for *2D HeLa* dataset that is 2.20% higher than the highest accuracy reported in (Nanni, et al., 2010c).

Table 11 Performance comparison with other published work

Method	*2D HeLa*	*LOCATE Endogenous*	*LOCATE Transfected*
(Hamilton, et al., 2007) 5F	-	98.2 (47)	93.2 (47)
(Chebira, et al., 2007) 5F	95.4 (78)	-	-
(Nanni and Lumini, 2008) 5F	94.2 (107)	98.4 (107)	96.5 (81)
(Nanni, et al., 2010c) 10F	97.5 (322)	-	-
(Nanni, et al., 2010a) 5F	95.8 (305)	99.5 (305)	97.0 (305)
SVM-SubLoc using *HarLBP*	**99.7** (581)	**99.8** (36)	98.5 (44)
SVM-SubLoc using *HarLTP*	**99.4** (78)	99.6 (62)	**98.7** (78)
SVM-SubLoc using *LTPs*	**99.0** (52)	95.6 (36)	93.6 (36)

5F and 10F represent 5-fold and 10-fold respectively

In addition, using *HarLBP* our approach has yielded the accuracy of 99.8% for LOCATE Endogenous dataset, which is 0.3% higher than the highest accuracy obtained by (Nanni, et al., 2010a). Similarly, using Har*LTP*, our approach achieved 98.7% accuracy for LOCATE Transfected dataset that is 1.7% higher than that of the proposed technique by (Nanni, et al., 2010a).

The performance of *SVM-SubLoc* approach is enhanced due to the two level ensembles; one is at the features level and the other is at the classifiers decision level. At features level, we have constructed the hybrid features by concatenating different individual feature sets. These features have improved the discrimination power of the features. At the classifiers decision level, we have combined the predictions of the utilized *SVMs* through the majority-voting scheme.

CONCLUSIONS

We have presented a simple, accurate, and effective prediction model for protein subcellular location images from *2D HeLa* and the two LOCATE datasets. The proposed *SVM-SubLoc* approach is reliable and computationally efficient. We have utilized both spatial and transform domain features. It has been shown that the performance of *SVM-SubLoc* is better compared to the individual classifiers using the hybrid features particularly *HarLBP* and *HarLTP* in spatial domain. The prediction accuracy has reached to 99.7% using *HarLBP* with features of 581 dimensions. On the other hand, the accuracy is 99.4% using *HarLTP* but the dimensionality of the feature space is reduced to 78 only, which is an effective reduction. These features are computationally more reasonable in terms of cost along with better discrimination capability compared to other texture based feature extraction strategies. In individual features, *LTPs* outperforms both hybrid and other individual features in terms of dimensionality of the feature space that is only 52. Even though the accuracy is 99.0%, which is a little less than that of *HarLBP*, it is preferable to use *LTPs* because of less computational cost. Additionally, these three feature sets have also performed well for the two LOCATE datasets. The hybrid features have brought a significant improvement in performance. This is due to the fact that the discrimination powers of both the feature spaces are utilized by *SVM-SubLoc*.

The comparative analysis highlights the improved performance of our proposed *SVM-SubLoc* approach in terms of both increased accuracy and reduced dimensionality of the feature space over existing well-known approaches.

ACKNOWLEDGEMENTS

This work is supported by the Higher Education Commission of Pakistan under the indigenous PhD scholarship program 17-5-4(Ps4-124)/HEC/Sch/2008/. We are also thankful to Dr. Loris Nanni Associate Researcher, Department of Information Engineering - University of Padua, Italy for his help in implementation.

CONFLICT OF INTEREST

The authors declare that they have no conflict of interest.

REFERENCES

Boland, M.V., Markey, M.K. and Murphy, R.F. (1998) Automated recognition of patterns characteristic of subcellular structures in fluorescence microscopy images, *Cytometry*, **33**, 366–375.

Boland, M.V. and Murphy, R.F. (2001) A neural network classifier capable of recognizing the patterns of all major subcellular structures in fluorescence microscope images of HeLa cells, *Bioinformatics*, **17**, 1213-1223.

Chebira, A., Barbotin, Y., Jackson, C., Merryman, T., Srinivasa, G., Murphy, R.F. and Kovacevic, J. (2007) A multiresolution approach to automated classification of protein subcellular location images, *BMC Bioinformatics*, **8**, 210.

Gunn, S.R. (1998) Support Vector Machines for Classification and Regression. Faculty of Engineering, Science and Mathematics, School of Electronics and Computer Science ,UNIVERSITY OF SOUTHAMPTON.

Hamilton, N.A., Pantelic, R.S., Hanson, K., Fink, J.L., Karunaratne, S. and Teasdale, R.D. (2006) Automated Sub-Cellular Phenotype Classification: An Introduction and Recent Results. *The 2006 Workshop on Intelligent Systems for Bioinformatics (WISB 2006)*. Australian Computer Society, Inc., Hobart, Australia, 67-72.

Hamilton, N.A., Pantelic, R.S., Hanson, K. and Teasdale, R.D. (2007) Fast automated cell phenotype image classification, *BMC Bioinformatics*, **8**.

Haralick, R.M. (1979) Statistical and Structural Approaches to Texture. *Proceedings of the IEEE*. 786-804.

Hayat, M. and Khan, A. (2010) Membrane Protein Prediction using Wavelet Decomposition and Pseudo Amino Acid based Feature Extraction. *Proceedings of the 6th IEEE International Conference on Emerging Technologies, (ICET 2010)*. 1-6.

Hu, Y. and Murphy, R.F. (2004) Automated interpretation of subcellular patterns from immunofluorescence microscopy, *Journal of Immunological Methods*, **290**, 93-105.

Khan, A., Majid, A. and Hayat, M. (2011) CE-PLoc: An ensemble classifier for predicting protein subcellular locations by fusing different modes of Pseudo amino acid composition, *Computational Biology and Chemistry*, **35**, 218-229.

Khan, A., Tahir, S.F., Majid, A. and Choi, T.-S. (2008) Machine learning based adaptive watermark decoding in view of an anticipated attack, *Pattern Recognition*, **41**, 2594-2610.

Lin, C.-C., Tsai, Y.-S., Lin, Y.-S., Chiu, T.-Y., Hsiung, C.-C., Lee, M.-I., Simpson, J.C. and Hsu, C.-N. (2007) Boosting multiclass learning with repeating codes and weak detectors for protein subcellular localization, *Bioinformatics*, **23**, 3374-3381.

Majid, A., Khan, A. and Mirza, A.M. (2006) Combining Support Vector Machines Using Genetic Programming, *International Journal of Hybrid Intelligent Systems* **3**, 109-125.

Murphy, R.F., Boland, M.V. and Velliste, M. (2000) Towards a Systematics for Protein Subcellular Location: Quantitative Description of Protein Localization Patterns and Automated Analysis of Fluorescence Microscope Images. *In Proceedings of the Eighth International Conference on Intelligent Systems for Molecular Biology*. AAAI Press, 251-259.

Murphy, R.F., Velliste, M. and Porreca, G. (2002) Robust Classification of Subcellular Location Patterns in Fluorescence Microscope Images. *Proceedings of the 2002 12th IEEE International Workshop on Neural Networks for Signal Processing*. 67-76.

Murphy, R.F., Velliste, M. and Porreca, G. (2003) Robust Numerical Features for Description and Classification of Subcellular Location Patterns in Fluorescence Microscope Images, *Journal of VLSI Signal Processing*, **35**, 311-321.

Nanni, L., Brahnam, S. and Lumini, A. (2010a) Novel Features for Automated Cell Phenotype Image Classification, *Advances in Computational Biology: Advances in Experimental Medicine and Biology (AEMB)*, **680**, 207-213.

Nanni, L., Brahnam, S. and Lumini, A. (2010b) Selecting the Best Performing Rotation Invariant Patterns in Local Binary/Ternary Patterns. *proceedings of the International Conference on Image Processing, Computer Vision, & Pattern Recognition (IPCV'10)*. Las Vegas, Nevada, USA, 369-375.

Nanni, L., Hsu, C.-N., Lumini, A., Lin, Y.-S. and Lin, C.-C. (2009) Automated cell phenotype image classification combining different methods. *Proceeding of the Workshop on Automated Interpretation and Modeling of Cell Images*. Montreal, Canada.

Nanni, L. and Lumini, A. (2008) A reliable method for cell phenotype image classification, *Artificial Intelligence in Medicine*, **43**, 87-97.

Nanni, L., Lumini, A., Lin, Y.-S., Hsu, C.-N. and Lin, C.-C. (2010c) Fusion of systems for automated cell phenotype image Classification, *Expert Systems with Applications*, **37**, 1556-1562.

Ojala, T., Pietikainen, M. and Harwood, D. (1996) A comparative study of texture measures with classification based on feature distribution, *Pattern Recognition*, **29**, 51-59.

Srinivasa, G., Merryman, T., Chebira, A., Kovacevic, J. and Mintos, A. (2006) Adaptive Multiresolution Techniques for Subcellular Protein Location Classification. *IEEE International Conference on Acoustics, Speech and Signal Processing*. 14-19.

Tan, X. and Triggs, B. (2007) Enhanced local texture feature sets for face recognition under difficult lighting conditions. *Proceedings of the 3rd international conference on Analysis and modeling of faces and gestures*. Springer-Verlag, Rio de Janeiro, Brazil, 168-182.